Inner limiting Membrane Peel Extends *In vivo* Calcium Imaging of Retinal Ganglion Cell Activity Beyond the Fovea in Non-Human Primate

Abbreviated Title: *In vivo* calcium imaging of retinal neurons beyond fovea

Hector C. Baez[1,2], Jennifer M. LaPorta[2], Amber D. Walker[2], William S. Fischer[2], Rachel Hollar[2,3], Sara Patterson[2], David A. DiLoreto Jr[2,3], Vamsi Gullapalli[3], Juliette E. McGregor[2,3]

1) Department of Biomedical Engineering, University of Rochester, Rochester, NY

2) Center for Visual Science, University of Rochester, Rochester, NY

3) Department of Ophthalmology, Flaum Eye Institute, University of Rochester Medical Center, Rochester, NY

Contact Author: Hbaez@ur.rochester.edu

Keywords

GCaMP, AOSLO, RGC, ILM Peel, Calcium Imaging, In-vivo, retinal imaging

Abstract

High resolution retinal imaging paired with intravitreal injection of a viral vector coding for the calcium indicator GCaMP has enabled visualization of activity dependent calcium changes in retinal ganglion cells (RGCs) at single cell resolution in the living eye. The inner limiting membrane (ILM) is a barrier for viral vectors, restricting transduction to a ring of RGCs serving the fovea in both humans and non-human primates (NHP). We evaluate peeling the ILM prior to intravitreal injection as a strategy to expand calcium imaging beyond the fovea in the NHP eye

in vivo. Five Macaca fascicularis eyes (age 3-10y; n=3 individuals; 2M, 1F) underwent vitrectomy and 5 to 6-disc diameter ILM peel centered on the fovea prior to intravitreal delivery of 7m8:SNCG:GCaMP8s. Calcium responses from RGCs were recorded using a fluorescence adaptive optics scanning laser ophthalmoscope. In all eyes GCaMP was expressed throughout the peeled area, representing a mean 8-fold enlargement in area of expression relative to a control eye. Calcium recordings were obtained up to 11 degrees from the foveal center. RGC responses were comparable to the fellow control eye and showed no significant decrease over the 6 months post ILM peel, suggesting that RGC function was not compromised by the surgical procedure. In addition, we demonstrate that activity can be recorded directly from the retinal nerve fiber layer. This approach will be valuable for a range of applications in visual neuroscience including pre-clinical evaluation of retinal function, detecting vision loss, and assessing the impact of therapeutic interventions.

Significance Statement

This research presents a groundbreaking advancement in visual neuroscience through the development of a novel technique involving the peeling of the inner limiting membrane (ILM) in conjunction with intravitreal injection to expand functional recording capabilities in the living primate eye. By utilizing high-resolution retinal imaging coupled with a viral vector-mediated expression of the calcium indicator GCaMP, the study achieves unprecedented visualization and assessment of retinal ganglion cell (RGC) activity at single-cell resolution. Importantly, the technique enables recording from regions of the retina previously inaccessible, significantly broadening the area for calcium imaging beyond the fovea. The results demonstrate stable RGC function post-procedure, suggesting minimal impact on retinal physiology. This innovative approach holds significant promise for diverse applications in visual neuroscience, including

pre-clinical evaluation of retinal function, detection of vision loss, and evaluation of therapeutic interventions. Overall, the study represents a major step forward in understanding and potentially treating retinal degenerative disorders, offering new avenues for research and development in vision restoration.

Acknowledgements

The authors would like to thank Qiang Yang for assistance with this study. The authors also thank the Penn Vector Core (RRID: SCR_022432) at the Perelman School of Medicine, University of Pennsylvania. Research reported in this publication was supported by the National Eye Institute of the National Institutes of Health under Audacious Goals Initiative funding award No. U24 EY033275 Accelerating photoreceptor replacement therapy with in-vivo cellular imaging of retinal function in primate, P30 EY001319 (core) and F32 EY032318 Foveal ganglion cell function in the living eye. The content is solely the responsibility of the authors and does not necessarily represent the official views of the National Inst. of Health. This study was supported by an Unrestricted Grant to the University of Rochester Department of Ophthalmology from Research to Prevent Blindness.

The authors declare no competing financial interests.

Introduction

Retinal degeneration is the leading cause of vision loss for adults in the industrialized world. Several approaches are under development to restore sight lost by retinal degenerative processes including cell-based therapies like photoreceptor transplantation (Lingam et al. 2021;

Aboualizadeh et al. 2020), viral vector based therapies like optogenetic restoration (Ferrari et al. 2020), and optoelectronic prostheses (Mathieson et al. 2012; Palanker et al. 2020). Use of small animal models, like mice, is often the first step in translating *in vitro* benchwork to human applications. However, non-human primates (NHP), endowed with visual and immune systems most analogous to humans, are the gold standard animal model to evaluate and optimize restored visual function and identify the most promising therapies for clinical trials.

The most comprehensive functional testing platform for model to restore vision would be capable of testing cellular scale resolution and connectivity throughout the living retina, but this ideal may not be practical. The most straightforward assessment of restored visual function have included behavioral tests such as light sensitivity testing (Hammer et al. 2022), optomotor assay (Lu et al. 2018), and water mazes (Batabyal et al. 2021). However, behavioral tasks alone cannot evaluate the quality of restored vision nor provide insights into methods to improve therapies. Multi-electrode array electrophysiology in retinal explants are widely used and allow for high temporal resolution of single-cell recordings, but is not fit for experiments observing long-term changes in retinal function (Gauvain et al. 2021; Ganjawala et al. 2019; Ferrari et al. 2020). Electroretinography measures broad photoreceptor response (Zhang, Su, et al. 2021), but lacks cell specificity and is less suitable for studies of vision restoration at the ganglion cell level (Nikonov et al. 2022).

Our model employs the use of adaptive optics imaging to help elucidate cellular function in our NHP model of visual restoration. Adaptive optics measures and corrects higher order aberrations of the eye to enable high-resolution imaging of *in vivo* retinal cells, such as photoreceptors and retinal ganglion cells (RGC) (Roorda et al. 2002; Aboualizadeh et al. 2020). Fluorescent imaging with genetically encoded calcium indicators enables the visualization of activity dependent calcium changes in neurons at the single cell and subcellular scale. The genetically encoded calcium indicator GCaMP is among the most widely adopted (Zhang et al.

2023). By pairing calcium imaging with an adaptive optics scanning laser ophthalmoscope (AOSLO), noninvasive single cell assessment of RGC activity becomes possible in the living primate eye (McGregor et al. 2020; McGregor et al. 2018; Yin et al. 2014). In this study, GCaMP8 is expressed in RGCs through an intravitreal injection of adeno associated virus (AAV) viral vector AAV2.7m8 (Dalkara et al. 2013) containing an SNCG (Chaffiol et al. 2017) ganglion cell promoter.

Despite successful expression of GCaMP in RGCs following intravitreal injection, viral transduction is limited to the parafoveal region in both humans and non-human primates (Comander et al. 2016). This has been linked to the inner limiting membrane (ILM), a thin border between the neural retina and vitreous fluid that is formed by astrocytes and the end feet of Müller cells, acting as a barrier to viral transduction (Dalkara et al. 2009). Since then, studies have demonstrated more widespread AAV-mediated transduction of GFP in retinal neurons by surgical peeling of the ILM from the retinal surface prior to intravitreal injection (Takahashi et al. 2017; Teo, Lee, and Constable 2018; Teo et al. 2018). However, this technique has yet to be applied to enable calcium imaging of RGC function in the living eye.

In this study we demonstrate that by pairing an ILM peel with virally induced GCaMP8 expression, it is possible to optically read out RGC function at single cell resolution from a significantly larger area of the living primate retina than previously possible. We also show the capability of GCaMP to functionally record the retinal nerve fiber layer (RNFL). Structural assessments were made using confocal scanning laser ophthalmoscopy (cSLO), optical coherence tomography (OCT), and color fundus photography. Single RGC functional assessments were made using AOSLO, granting a previously unexplored cellular scale perspective on the impact of ILM peels on the retina. This new perspective may be useful for studies investigating ILM peels applied as a part of treatment in humans (Brooks 2000; Dera et al. 2023) or glaucoma stem cell therapy (Leffler et al. 2023).

Materials and Methods

Experimental Design

In this study, five experimental eyes and one control eye of macaques were used. All five experimental eyes were vitrectomized and underwent peeling of the ILM centered on the fovea (Figure 1A-B). Six to eight weeks later intravitreal injection of a viral vector was performed to produce GCaMP expression in the ganglion cell layer (Figure 1C). Four of the six eyes received intravitreal injection of viral vector AAV2.7m8-SNCG-GCaMP8s while the two eyes of macaque M3 received the GCaMP8m variant. One control GCaMP8s eye did not undergo ILM peeling (Table 1). The viral vector led to robust expression of calcium-level dependent fluorescent protein within RGC after two months. Scanning laser ophthalmoscopy (cSLO) confirmed the presence of GCaMP in the area corresponding to region of ILM peeling surgical peel (Figure 1D). cSLO, OCT, and color fundus photography were performed longitudinally up to six months post procedure. Functional assessment at the cellular scale was conducted using AOSLO in combination with a red LED flashing stimulus (Figure 1E-G). Retinal imaging was conducted between the fovea and the ILM peel edge in all meridians, signifying the limit of fluorescence expression.

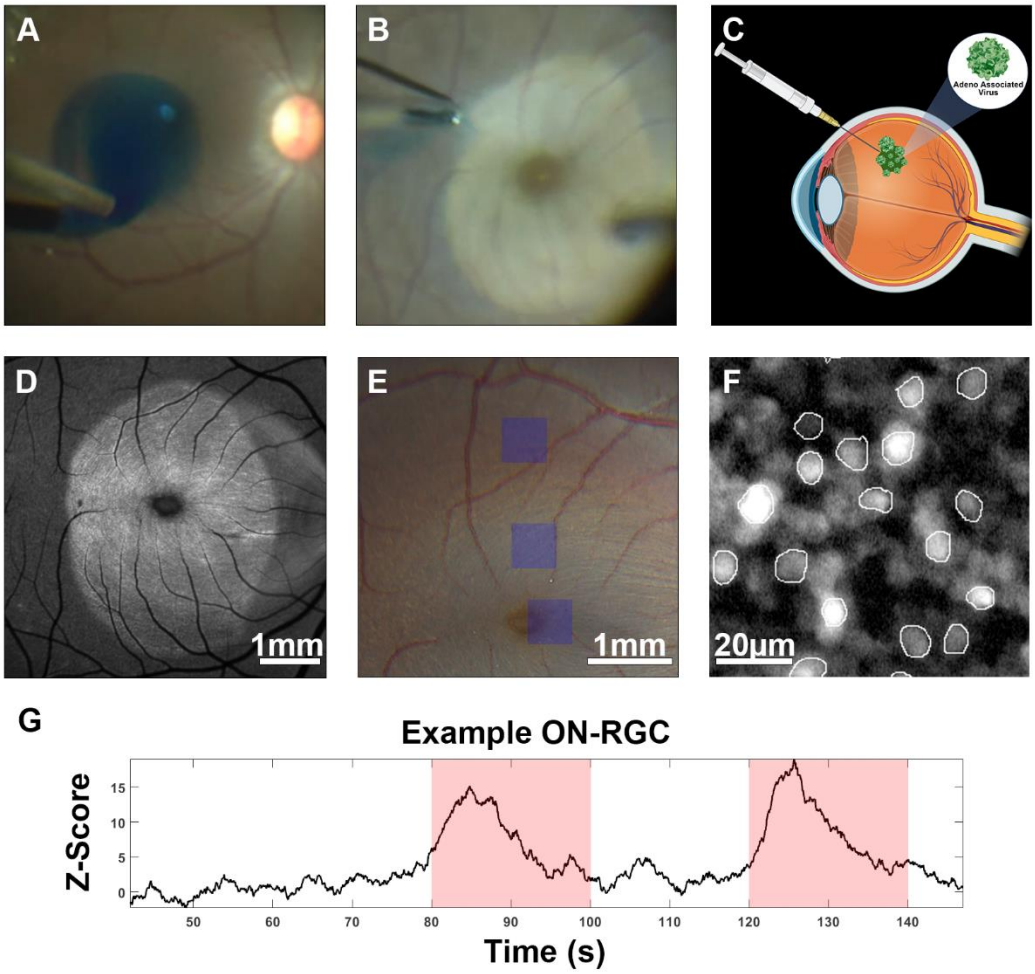

Figure 1 ILM Peeling enables AAV-mediated fluorescence beyond the fovea in macaque

A. Following a pars plana vitrectomy, the ILM is stained with brilliant blue dye. **B.** Mechanical force lifts the ILM in a circular pattern around the fovea using forceps. **C.** Intravitreal injection delivers viral vector to the retina. **D.** A blue autofluorescence (BAF) confocal scanning laser ophthalmoscope (cSLO) confirmed the presence of GCaMP in a pattern matching the surgical peel two months post injection. **E.** Functional assessments were conducted at retinal imaging locations in using a blue 488nm excitation source in combination with a red LED flashing stimulus. **F.** Individual RGCs were segmented and **G.** their responses to the LED stimulus tabulated.

Macaque (eye)	*sex*	Age at time of ILM peel	Inactivating antibodies to AAV2	Time between immune suppression and ILM peel (days)	Time between ILM peel and viral vector Injection (days)	Time of AAV2 injection after initial injection in fellow eye (days)	GCaMP Variant
M1 (OS)	*M*	Control	1:4	Control	Control	---	GCaMP8s
M1 (OD)		10y 9m		31	28	29	GCaMP8s
M2 (OS)	*M*	4y 2m	1:5	27	50	41	GCaMP8s
M2 (OD)		4y 3m		62	55	---	GCaMP8s
M3 (OS)	*F*	3y 10m	1:10	98	42	35	GCaMP8m
M3 (OD)		3y 11m		126	48	---	GCaMP8m

Table 1: Summary of demographic and experimental parameters for all eyes involved in the study.

The sex and age of the primate, immune suppression status quantity and type of viral vector injected intravitreally, and the time elapsing between the ILM peel and the intravitreal injection in days is listed for each eye.

Animal welfare

The macaques used in this study were housed in pairs in an AAALAC accredited facility in compliance with the University of Rochester University Committee on Animal Resources (UCAR). They had free access to water and primate biscuits, providing a complete and nutritious diet. To supplement this, they were given various treats multiple times daily, such as nuts, dried fruit, vitamin chews, and a large variety of fresh fruits and vegetables. They were

also given “high value” treats during training, including Ensure, marshmallow snacks, and fruit gummies. An animal behaviorist and Veterinary Technicians provided novel enrichment items multiple times a week, including items such as grass, oranges with peels still on, treat filled forage boxes, grapevines, water play, and popcorn balls. Daily enrichment included mirrors, puzzle feeders, durable chew toys, daily television time and/or music and regular visits from staff to offer treats and socialization. All macaques were cared for by the Department of Comparative Medicine veterinary staff, including three full-time Veterinarians, five Veterinary Technicians, and an animal care staff who monitored animal health and comfort at least three times daily. The Animal Behaviorist regularly recorded and analyzed primate behavior to monitor any signs of stress. This study was carried out in strict accordance with the Association for Research in Vision and Ophthalmoscopy (ARVO) Statement for the Use of Animals and the recommendations in the Guide for the Care and Use of Laboratory Animals of the National Institutes of Health. The protocol was approved by the University Committee on Animal Resources of the University of Rochester (PHS assurance number: D16-00188(A3292-01)).

Immunosuppression

All macaques in this experiment received subcutaneous Cyclosporine injections daily. Blood trough levels were collected to titrate the dose of 150-250 ng/mL and then maintained at that level. The timing of immune suppression relative to ILM peel surgery and viral vector injections are detailed in Table 1.

Animal preparation for ILM peel surgery

The surgical subject was fasted overnight with free access to water. The animal was sedated using ketamine (100mg/mL) and medetomidine (20mg/mL), then intubated and kept at proper

anesthetic depth via 1.5-3% isoflurane throughout the procedure. The animal was positioned in dorsal recumbency on a padded surgical table. A Bair Hugger warming system was placed over the animal to maintain body temperature. Vital signs including temperature, heart rate and rhythm, respirations, end tidal CO2, blood pressure, SpO_2, and reflexes were monitored consistently and recorded every fifteen minutes. Pupil dilation was accomplished using 1% atropine ophthalmic solution. An aseptic preparation was performed on the surgical eye and surrounding area using 5% betadine solution and flushed with sterile 0.9% saline. The subject's eye and body were then draped in a sterile fashion.

ILM Peel procedure

The ILM peel procedures performed in NHP closely followed the process used in human surgery. A standard 3-port pars plana vitrectomy was performed through 25-gauge cannulas using the Constellation vitrectomy system (Alcon, Ft. Worth, TX), OPMI Lumera 700 operating microscope, and RESIGHT viewing system (Carl Zeiss Meditec AG, Jena, Germany). Triamcinolone was injected intravitreally to enhance visualization of the vitreous. A posterior vitreous detachment was induced using aspiration from the vitrector or a soft tip cannula. The peripheral vitreous was trimmed. Brilliant Blue G Ophthalmic Solution (DORC) was placed over the macula and the ILM stained for 2 minutes (Supplementary Movie 1). A fluid-fluid exchange was performed to remove the dye. The stained ILM was then peeled 360 degrees, centered on the fovea, in approximately 5 to 6-disc diameter area in the macula using ILM peeling forceps (Alcon, Ft. Worth, TX) (Supplementary Movie 2). The three ports were then removed at the end of the surgery and the sclerotomies sutured. The animal was given an intravitreal injection of vancomycin (1mg/0.1mL) and ceftazidime (2mg/0.1mL). Immunosuppressant Cyclosporine (150-250ng/mL), anti-inflammatory meloxicam (5mg/mL), analgesic buprenorphine SR

(3mg/mL), and an anesthetic reversal of antisedan (5mg/mL) were all administered post-operatively.

Intravitreal Injection of viral vector

Intravitreal injection of AAV2-7m8.SNCG.jGCaMP8s.WPRE.SV40 (100 μL at titer 2.62×10^{13} GC/mL), or AAV2-7m8.SNCG.jGCaMP8m.WPRE.SV40 (100 μL at titer ≥ 2.46×10^{13} GC/mL), was performed as previously described in Yin et al 2011 (Yin et al. 2011). Briefly, the eye was sterilized with 5% diluted betadine before the vector was injected into the vitreous through the pars plana using a tuberculin syringe and 30-gauge needle. All viral vectors were synthesized by the University of Pennsylvania Vector Core. Neutralizing antibodies to AAV2 were 1:25 or lower in all four injected animals prior to the study. Following the intravitreal injection of the vector, each eye was imaged weekly with a conventional scanning light ophthalmoscope (Heidelberg Spectralis, Heidelberg Engineering, Franklin, MA) using the 488 nm autofluorescence modality, to determine the onset of expression, image quality and to monitor eye health. The animal received 2mg/0.05mL of triamcinolone intravitreally (Kenalog-40) following the injection to treat for symptoms of uveitis.

Animal preparation for imaging

All monkeys were fasted from 4 to 18 h prior to anesthesia induction. Anesthesia induction began with 5 to 20 mg/kg Ketamine, 0.25 mg/kg Midazolam, and 0.017 mg/kg Glycopyrrolate intramuscularly. The pupil was dilated with a combination of tropicamide 1% and phenylephrine 2.5%. In cases of minimal pupil dilation within the standard time, phenylephrine 10% and/or cyclopentolate 1% drops were administered. Flurbiprofen Ophthalmic drops are given to the

target eye, to prevent any discomfort from prolonged use of an eye lid speculum. Both eyes were covered with a hydrating ophthalmic gel (GenTeal). The target eye then had the lid speculum placed to keep the eye open during imaging and a contact lens was placed to ensure corneal protection. The fellow eye was taped closed with porous tape, to protect the cornea from drying.

The animal was placed in a stereotaxic cart. Prior to intubation, an oxygen mask with 1–2% isoflurane, was placed over the monkey's face to allow for adequate sedation for intubation. An intravenous drip of Ringer's lactate with 5% dextrose was maintained at 5 ml/kg/hr for the duration of imaging. The monkey was intubated and maintained at a surgical plane of anesthesia with isoflurane 1.0–2.5%. A Bair Hugger warming system was placed over the monkey to maintain body temperature. Monitoring was conducted as previously described.

After a surgical plane of anesthesia had been established, a Rocuronium infusion (800mcg/ml) was given with a dose range from 200-600mcg/kg/hr, after an initial bolus dose of 100-400mcg/kg. Rocuronium is administered to effect, determined by eye movement, and the lowest effective dose per animal is used. Once respirations ceased, the monkey was maintained on a ventilator until imaging was over and the infusion was turned off. Once a peripheral nerve response was established, an intravenous dose of glycopyrrolate 0.01 mg/kg was given. Five minutes after the glycopyrrolate, neostigmine 0.05 mg/kg was given intravenously. The monkey was monitored for indications of breathing against the ventilator and then removed from the ventilator once able to breath without assistance. The monkey was removed from the isoflurane no sooner than fifteen minutes after the neostigmine injection to ensure stability off the ventilator. The monkey was then allowed to wake up and extubated once all reflexes had returned.

Clinical imaging

Confocal scanning light ophthalmoscopy (cSLO), optical coherence tomography (OCT) and color fundus photography were performed to pre- and post-procedure using a commercially available Spectralis HRA (Heidelberg Engineering) and fundus camera (Topcon 50EX). The blue autofluorescence modality was used to capture GCaMP fluorescence using the 488nm excitation wavelength and a longpass filter at 500nm. 30- and 55-degree OCT images centered on the fovea were collected pre- and post-ILM peel, pre-and post-intravitreal injection, and roughly every 30 days thereafter. OCT data from the optic nerve head in addition to slit lamp photographs (Zeiss) were recorded at the same timepoints to document the time course and severity of any inflammation.

Assessing ocular inflammation

A modified Hackett-McDonald scoring system (Munger 2002) was used to evaluate ocular inflammation. Veterinary technicians evaluated the pupil reflex and conjunctival discharge prior to pupil dilation. Slit lamp images were randomized and graded by an ophthalmologist (VG). The scoring system is available in the supplementary materials.

Adaptive Optics Scanning Laser Ophthalmoscope Imaging

Adaptive Optics Calcium imaging was collected using a previously described AOSLO instrument (Gray et al. 2006; Godat et al. 2022). An 847nm diode laser (QPhotonics, 100-136uW/mm2) was used as a wavefront sensing beacon in combination with a Shack-Hartman wavefront sensor and a deformable mirror (ALPAO) for measuring and correcting the optical aberrations of the eye. Briefly, a 796nm superluminescent diode (Superlum, 700-850uW/mm^2) was used to

image the cone photoreceptor layer using a 2 airy disc (20um) pinhole. A 488nm laser (Qioptiq, 57uW/mm2) focused on the RGC layer excited the fluorophores for GCaMP imaging through a 7.5 airy disc (75um) pinhole and was collected simultaneously with the photoreceptor reflectance video. Laser powers were calibrated prior to every imaging session to ensure consistency across sessions. To correct for longitudinal chromatic aberration between the 796nm source and 488nm sources on the detector, motorized stages were optimized to the best focal and lateral positions prior to each experiment. The adaptive optics control facilitated fine focus on the retinal ganglion layer at each 2.54° by 2.54° retinal location. Trials began with a 60 second system background period with no laser emission. Next, the cells were adapted to the mean luminance of the 488nm source emission over a 120 second period. A fluorescence background was captured during this period of constant illumination. GCaMP fluorescence (emission 535/20 nm) was recorded in response to visual stimuli presented through a Maxwellian view system (Baron 1973). A 661nm ± 20 nm LED was used to avoid the GCaMP excitation spectrum., while. The stimulus consisted of 20 second contrast increments and decrements against a mean light level (3 μW/mm^2). Each trial was repeated twice at each retinal location. Total exposure to all laser sources was kept below the Rochester exposure limit (Rossi et al. 2013), designed to be two-fold more conservative than the ANSI standard (Thomas et al. 2007).

Data Analysis

Adaptive optics calcium imaging was stored as an uncompressed AVI video format. A frame-by-frame stimulus record was written to a csv file, providing an accurate for analysis. The reflectance videos of the photoreceptor mosaic were registered offline using a strip-based cross correlation algorithm (Yang et al. 2014), which corrected the translations between frames and intraframe warping due to eye movement in the photoreceptor reflectance video. Each frame of

the GCaMP fluorescence video was also co-registered to the photoreceptor reflectance video. The frames of the fluorescence video were temporally integrated to form a high SNR z projection image to create an RGC segmentation mask. A background subtraction was performed to better visualize individual RGCs. RGC segmentation masks were imported into MATLAB and used to tabulate individual cell traces for each imaging location. These cell traces were then filtered using a 50-frame moving median filter. The Z-score was calculated as the GCaMP response amplitude (signal) minus the mean amplitude of the baseline adapted response (noise), all divided by the standard deviation of the noise. The criterion for a responsive cell was set to 2.5 standard deviations above the noise. Statistical analyses were performed using MATLAB two-sample T-test, with group spread reported as mean ± SD. Fluorescence cSLO images were scaled analyzed using FIJI to determine the fluorescence boundaries.

Code and Data Accessibility

All code used for analysis and corresponding filtered RGC recordings will be made available on our GitHub and the open science framework repository upon publication. Raw video data is available upon request.

Results

ILM peel enables functional recording from RGCs at previously inaccessible eccentricities *in vivo*

To assess the impact of ILM peel on the spatial extent of GCaMP transduction in the GCL we directly compared the pattern of expression in the ILM peeled eye with the fellow eye of the

same animal (MX) which received an in intravitreal injection but no ILM peel (control). Figs 2A and 2B show a dramatic 5-fold increase in the area of GCaMP expressing RGCs in the ILM peeled eye (12.9mm^2) relative to the control (2.5 mm^2). In the ILM peeled eye RGCs were transduced with GCaMP out to 9.2 degrees superior to the fovea whereas in the control eye the maximum eccentricity was just 3.5 degrees. The fluorescence extended to the limit of the surgical peel.

To assess the responses of RGCs in the ILM peeled and control eye we performed calcium imaging AOSLO while the retina received periodic visual stimulation at 0.025Hz. Figure 1G shows an example fluorescence trace from a single ON cell in the ILM peeled eye. The magnitudes of single cell responses recorded in the ILM peeled and control eyes are shown in Figure 2C represented as z-scores. The distribution of z-scores from individual RGCs in the ILM peeled and control eyes were not significant at 1° (P=0.07) or 3.5° (P=0.61), suggesting that the ILM peel did not adversely impact RGC physiology. Importantly only in the ILM peeled eye was it possible to obtain functional recording from RGCs at eccentricities beyond 3.5 degrees. Figure 2C shows responses collected from RGCs at 9.2 degrees from the foveal center. This is the first-time *in vivo* calcium imaging has been performed outside the parafovea. No RGCs fluoresced at 9 degrees from the fovea in M1 OS. Z-scores from M1 OD at 9.2 degrees were found to be significantly lower those at 3.5 degrees in the same eye (P=0.0004).

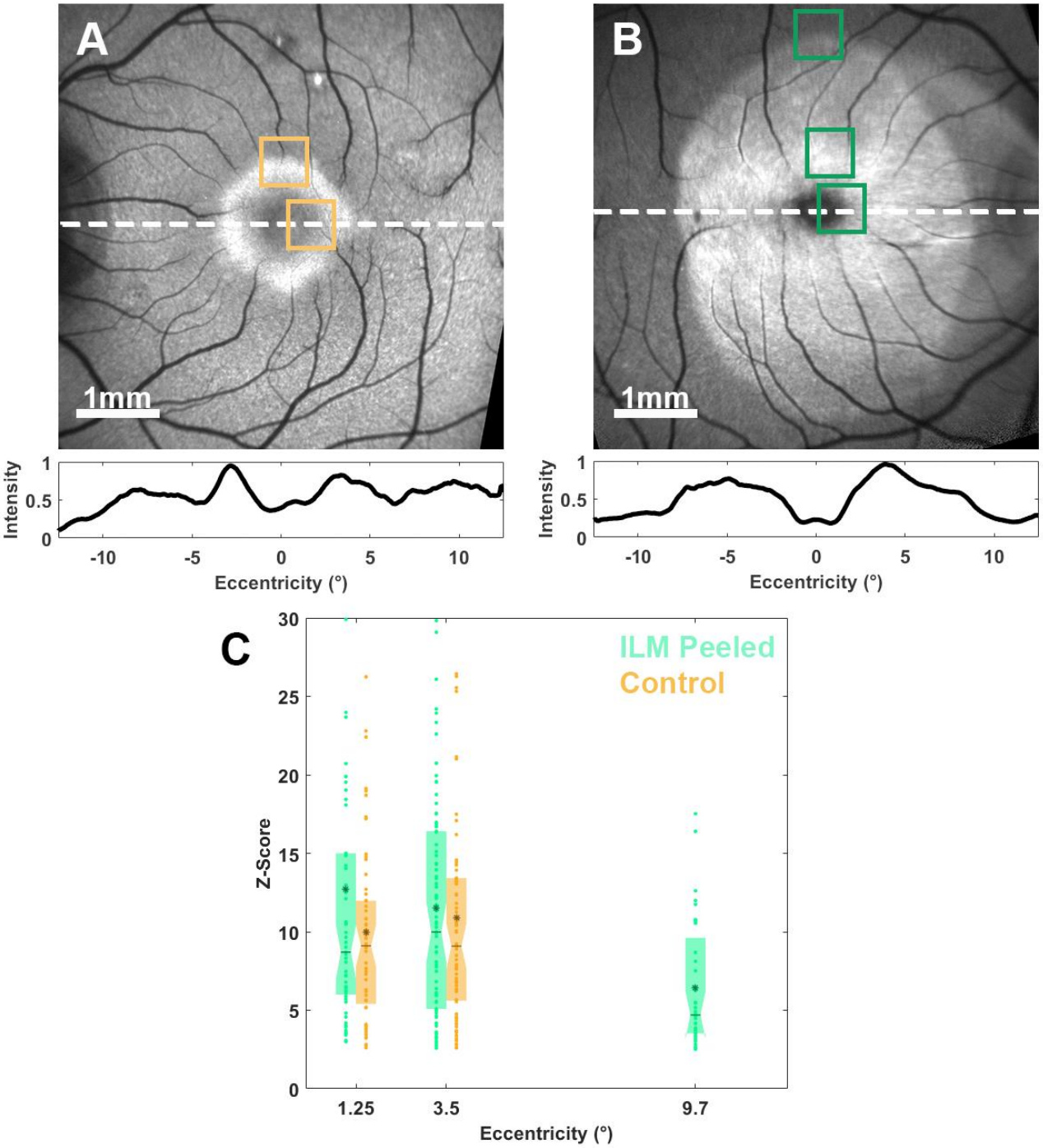
A
1mm
B
1mm
Intensity
1
0.5
0
-10
-5
0
5
10
Eccentricity (°)
C
ILM Peeled
Control
Z-Score
30
25
20
15
10
5
0
1.25
3.5
9.7
Eccentricity (°)

Figure 2

A. 30°cSLO BAF images centered on the fovea, taken in each eye of M1 including the A control eye OS and **B.** the ILM peeled eye OD. GCAMP Fluorescence intensity contour (visualized in lower panel, line denoted by white dashed line) is normalized to max value and smoothed. AOSLO Imaging locations are labeled for each eye. **C.** Box plot of individual RGC Z-scores at each imaging location, grouped by retinal eccentricity. Group responses are 12.7 ± 10.4, n=67; 10.0 ± 6.6, n=62; 11.52 ± 7.5, n = 85; 10.9 ± 7.6; n = 73; 6.4 ± 3.9, n=40, respectively. Taken at 17 weeks post intravitreal injection in OS and 21 weeks OD.

RGC remain responsive for at least 6 months after ILM peel

As functional recordings were obtained *in vivo* it was possible to return to the same region of the GCL to longitudinally monitor RGC responses over a period of months as shown in figure 3. RGC amplitudes at 9 degrees did not significantly change over time (paired t test; P=0.86, P=0.42), but the amplitudes at 3 degrees significantly increased after 5 months (paired t test; P=0.02).

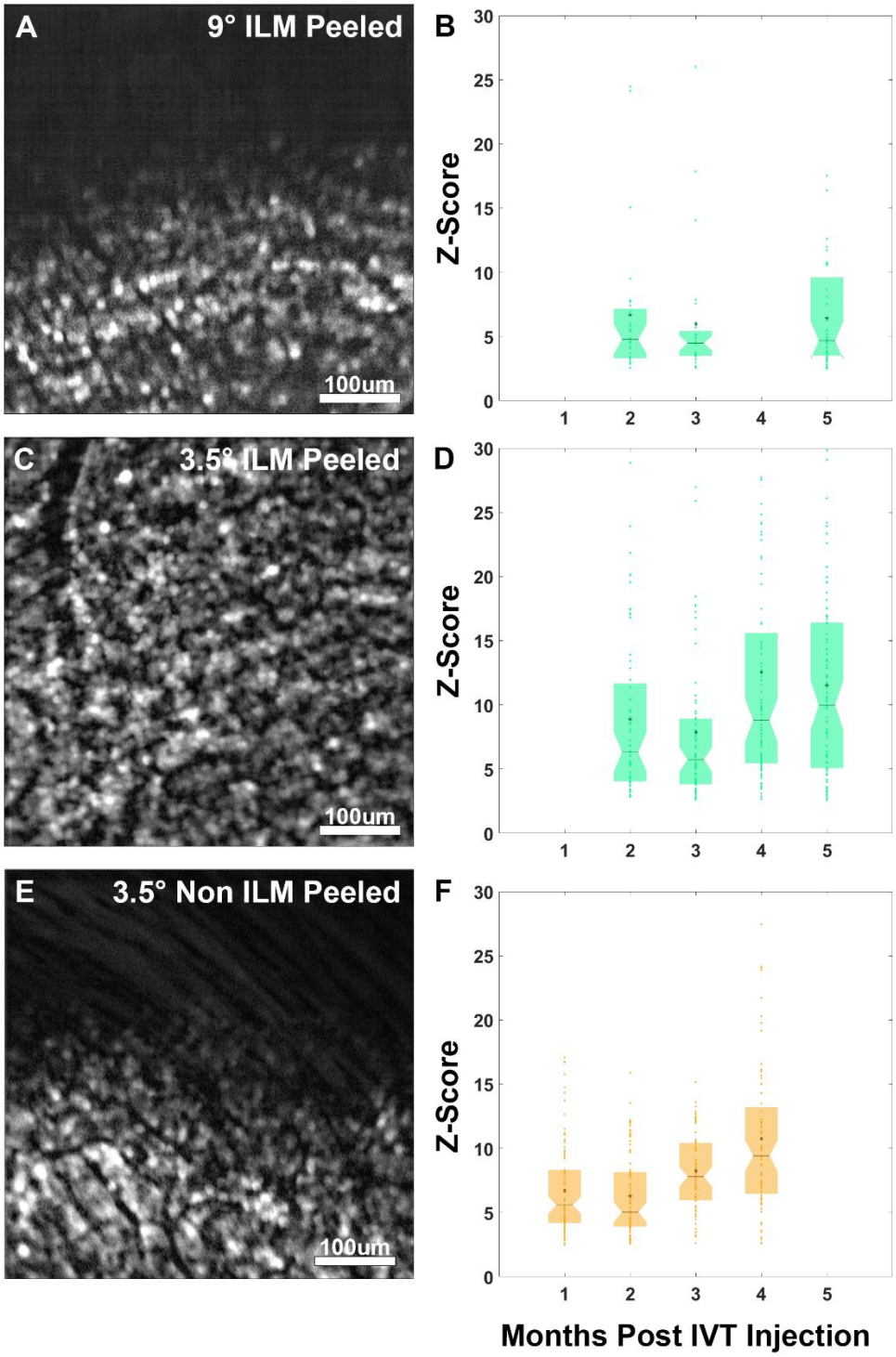
A
9° ILM Peeled
100um
B
C
3.5° ILM Peeled
100um
D
E
3.5° Non ILM Peeled
100um
F
Z-Score
0
5
10
15
20
25
30
1
2
3
4
5
Months Post IVT Injection

Figure 3

A. AOSLO GCaMP time-integrated image used to create segmentation masks at the edge of the ILM peeled area at 9° from the fovea of M1 OD. **B.** Responses at two (6.7 ± 5.7,n=27), three (6.0 ± 5.2,n=28), and five (6.4 ± 4.0,n=40) months post intravitreal injection, or three, four, and six months post ILM peel. **C.** AOSLO GCaMP image within the ILM peeled area at 3.5° from the fovea of M1 OD. **D.** Responses at three (8.9 ± 6.2,n=59), four (7.8 ± 6.6,n=68), five (12.5 ± 10.2,n=87), and six (11.5 ± 7.5,n=76) months post intravitreal injection. **E.** AOSLO GCaMP image of the non-peeled eye at 3.5° from the fovea of M1 OS. **F.** Responses at one (6.7 ± 3.5,n=97), two (6.3 ± 3.2,n=74), three (8.2 ± 2.9,n=81), and four (10.7 ± 6.0,n=75) months post intravitreal injection.

RGC response amplitudes measured in all eyes

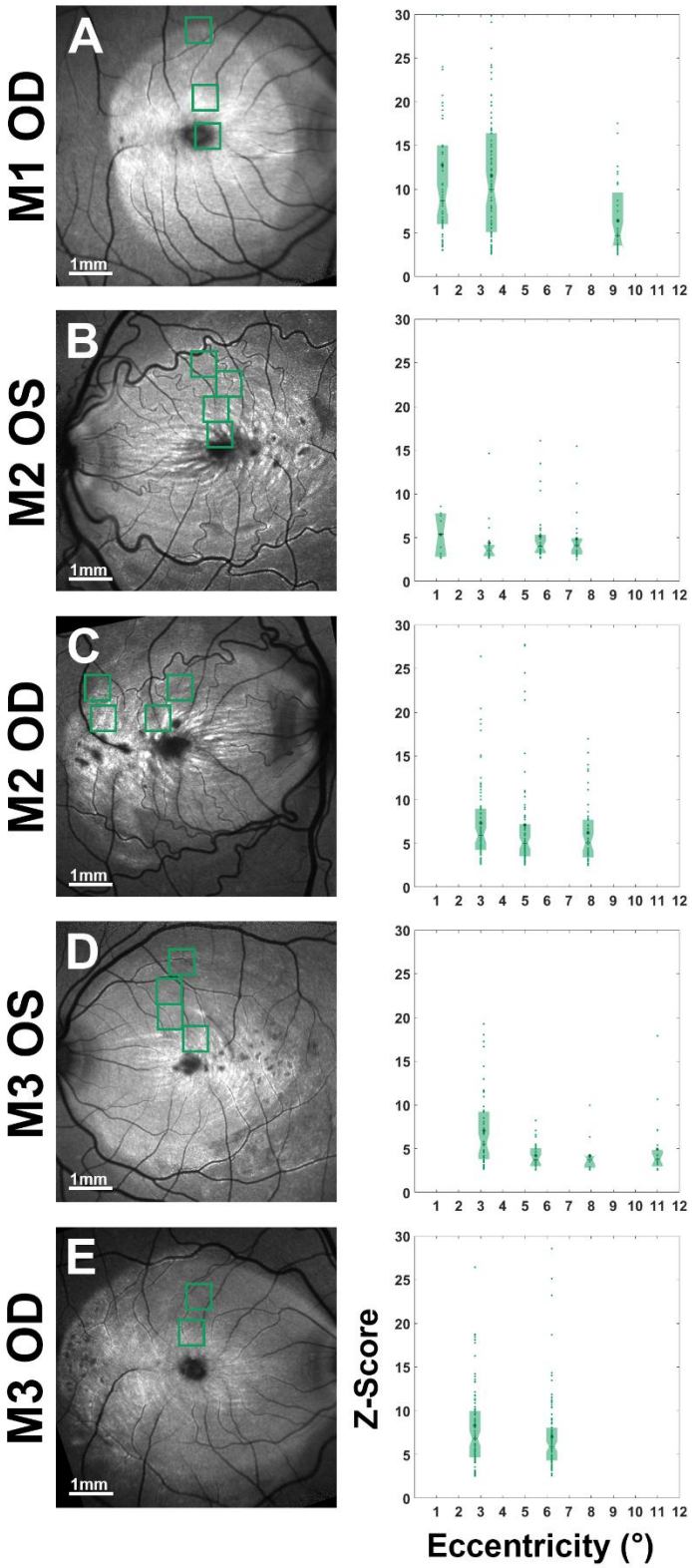

Figure 4: RGC response amplitudes measured in all eyes

A. (left) 30°cSLO BAF images centered on the fovea for all experimental eyes, imaging locations shown with blue squares. (right) Individual RGC Z-scores in box plots for M2 OD (12.7 ± 10.4,n=67, 11.5 ± 7.5,n=85, and 6.4 ± 3.95,n=40) taken five months post IVT injection, **B.** M2 OS (5.4 ± 2.5,n=12, 4.4 ± 2.9,n=17, 5.2 ± 3.3,n=30, and 4.4 ± 3.0,n=24) taken three months post IVT injection, **C.** M2 OD (7.3 ± 4.6,n=81, 7.1 ± 6.2,n=77, and 6.2 ± 3.7,n=48) taken five months post IVT injection, **D.** M3 OS (7.1 ± 4.3,n=52, 4.2 ± 1.5,n=31, 4.2 ± 2.1,n=12, and 4.9 ± 3.6,n=20) taken five months post IVT injection, **E.** M3 OD (8.3 ± 6.4,n=92, and 7.1 ± 4.4,n=99) taken six months post IVT injection.

An additional 4 eyes underwent ILM peeling prior to intravitreal injection and imaging, finding an average 8-fold increase in area (12.9mm^2, 24.4 mm^2, 20.1 mm^2,22.7 mm^2, 20.7 mm^2, respectively) of GCaMP expression across all eyes relative to the control eye (2.5mm^2) as measured using BAF cSLO (Figure 4). We extracted functional activity from RGCs in all eyes at eccentricities out to 9.2, 7.4, 7.9, 11, and 6.2 degrees respectively. There was a significant decrease in response magnitude with eccentricity in between the smallest and largest retinal eccentricities of M1 OD (p=0.0003). This pattern was not repeated in M2 OS (p=0.598), M2 OD (p=0.147), M3 OS (p=0.055), and M3 OD (p=0.122). Since both GcAMP8s and GcAMP8m were used in this study, we also sought to compare response magnitudes between those eyes. Responses between M1 OD (GCAMP8s) were significantly higher than M3 OS (GCAMP8m, p= p=0.001) and OD (GCAMP8m, p=0.001) at similar eccentricities but M2 (GCAMP8s) were not statistically significant for OS (p= 0.12) or OD (p=0.20). We note that M2 had naturally occurring vessel tortuosity.

Optical readout of RGC activity is possible from the retinal nerve fiber layer

For the first time we show that it is possible to record not only from RGC somas but also from the RNFL near the optic disc (figure 5). We evaluated RNFL calcium responses in both the ILM peeled and control eye. The investigated locations lack fluorescing RGC somas but contained GCaMP expressing axonal fibers. Although individual fibers could not be functionally separated, integrating over a large area enables extraction of population-level responses. The averaged signal corresponded to an 'OFF' type response in both cases, but in the control eye the magnitude of the response was reduced by half. This is consistent with there being more labelled RGCs in the ILM peeled eye. (3.3 ± 0.02, and 1.4 ± 0.02, respectively).

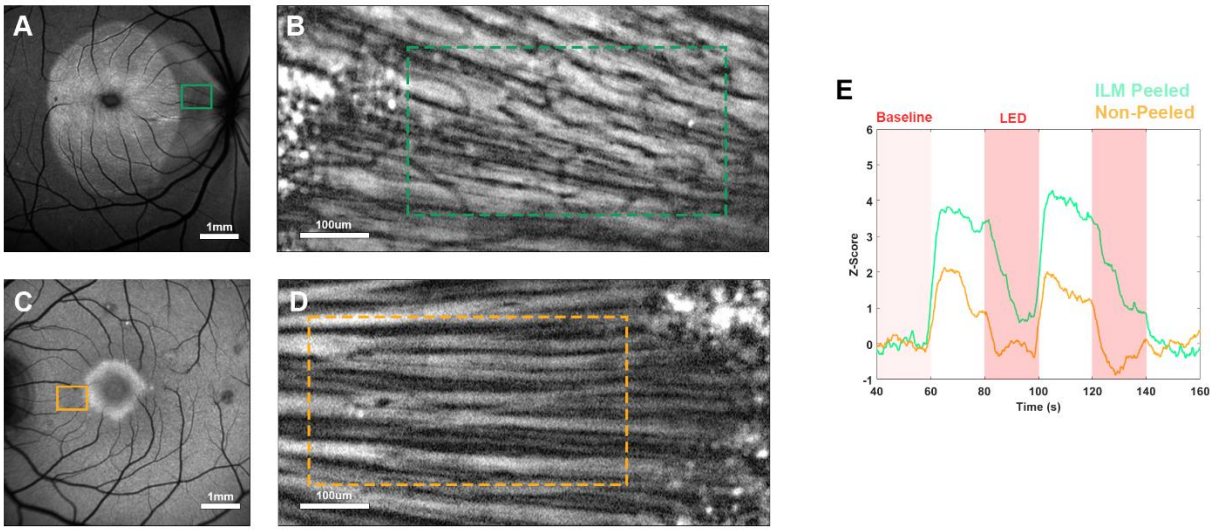

Figure 5: Optical readout of RGC activity from the retinal nerve fiber layer

A. 30°cSLO BAF images centered on the fovea of M1 OD (ILM-peeled). **B.** AOSLO GCaMP time-integrated image taken at the Nasal region shown in M1 OD. The green dotted line represents an area-integration used to construct a temporal signal for these RNFL bundles **C.** 30°cSLO BAF images centered on the fovea of M1 OS (non-peeled). **D.** The orange dotted line

represents an area-integration used to construct a temporal signal for these RNFL bundles **E.** RNFL area-integrated traces responding to an OFF-onset of the LED stimulus at 60s and 100s (Z-Score responses 3.36 ± 0.02, and 1.45 ± 0.02, respectively), filtered using moving median filter as previously described.

Structural imaging reveals minor morphological changes following ILM peel

To ensure we had a full understanding of any structural changes in the retina occurring because of the ILM peel, we closely monitored all eyes over time with fundus photography and OCT (Figure 6). As reported in previous studies darkened spots appeared surrounding the fovea in three out of five eyes. These concentric macular dark spots (CMDS) (Alkabes et al. 2011), appear as stretch marks in the direction of the optic nerve fibers. We note an alteration of the foveal contour in the B-scan OCT images of all subjects occurring to a variable extent amongst individuals. The foveal pit diameter of M1 OD and M3 OD appears reduced compared to pre-ILM peel. In contrast, the foveal contours of M2 OS and M3 OS are more dramatically altered. These changes in foveal contour persist throughout the observation period (6 months post ILM peel). No macular holes were created but disruption to the photoreceptor layer was noted in M2 OS which appeared to improve over time.

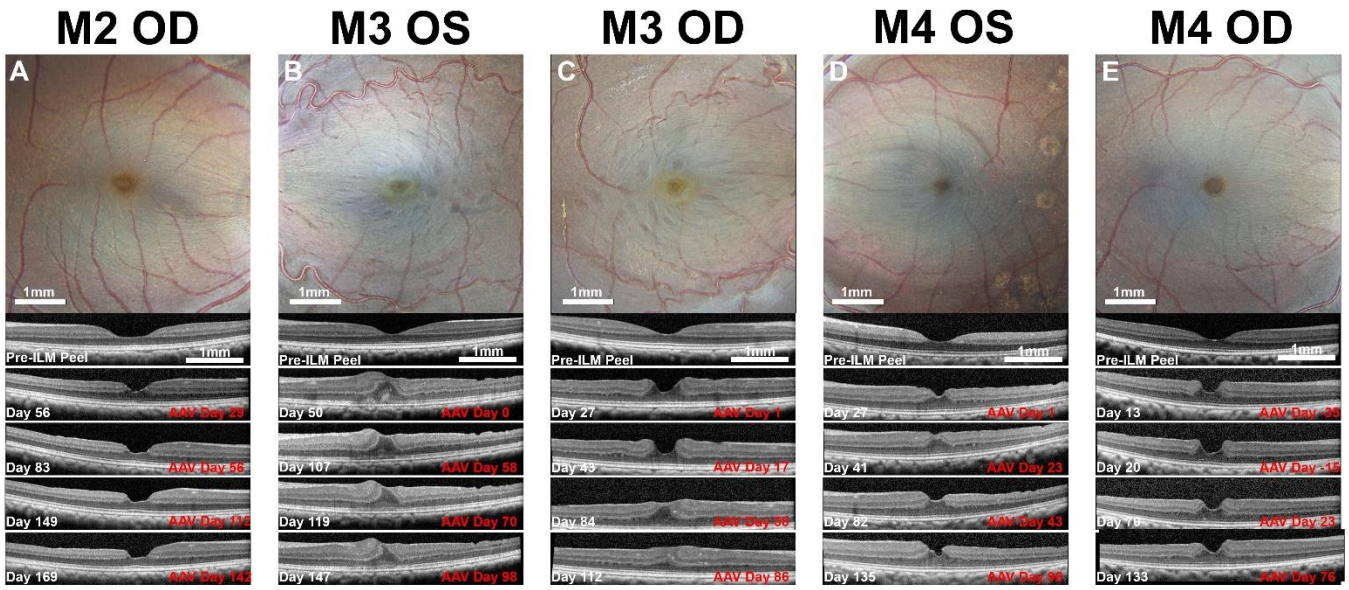

Figure 6: Structural imaging reveals minor morphological changes following ILM peel

A-E (top) 55° Color fundus images of all ILM peeled eyes centered on the fovea and taken two-months post ILM peel. (bottom) B-scan OCT images taken between 2-24 weeks post ILM peel procedure. Note M4 OS has localized patches of outer retinal damage temporal to the macular that are unrelated to the present study.

To further investigate CMDS, we correlated B-scan OCT, color fundus and fluorescence cSLO data with and AOSLO images over the regions of interest. cSLO and AOSLO calcium imaging confirm the presence of hypofluorescent areas within some CDMS regions visible in the color fundus, implying an absence of RGCs (Figure 7A-C). B-Scan OCT images reveal shallow dimples in the RNFL, reported previously as disassociated optical nerve fiber layer (DONFL) (Tadayoni et al. 2001; Christensen et al. 2009). M1 OD despite having no CMDS markers visible in the color fundus was found to have one hyperfluorescent region near the edge of expression (Figure D-E). However, not all CDMS seen in the fundus are visible in the OCT or AOSLO

modalities. For M2 OD (Figure 7F-G), we show one CDMS region that does not appear on the OCT or AOSLO. These hypofluorescent areas appear mostly in the temporal retina.

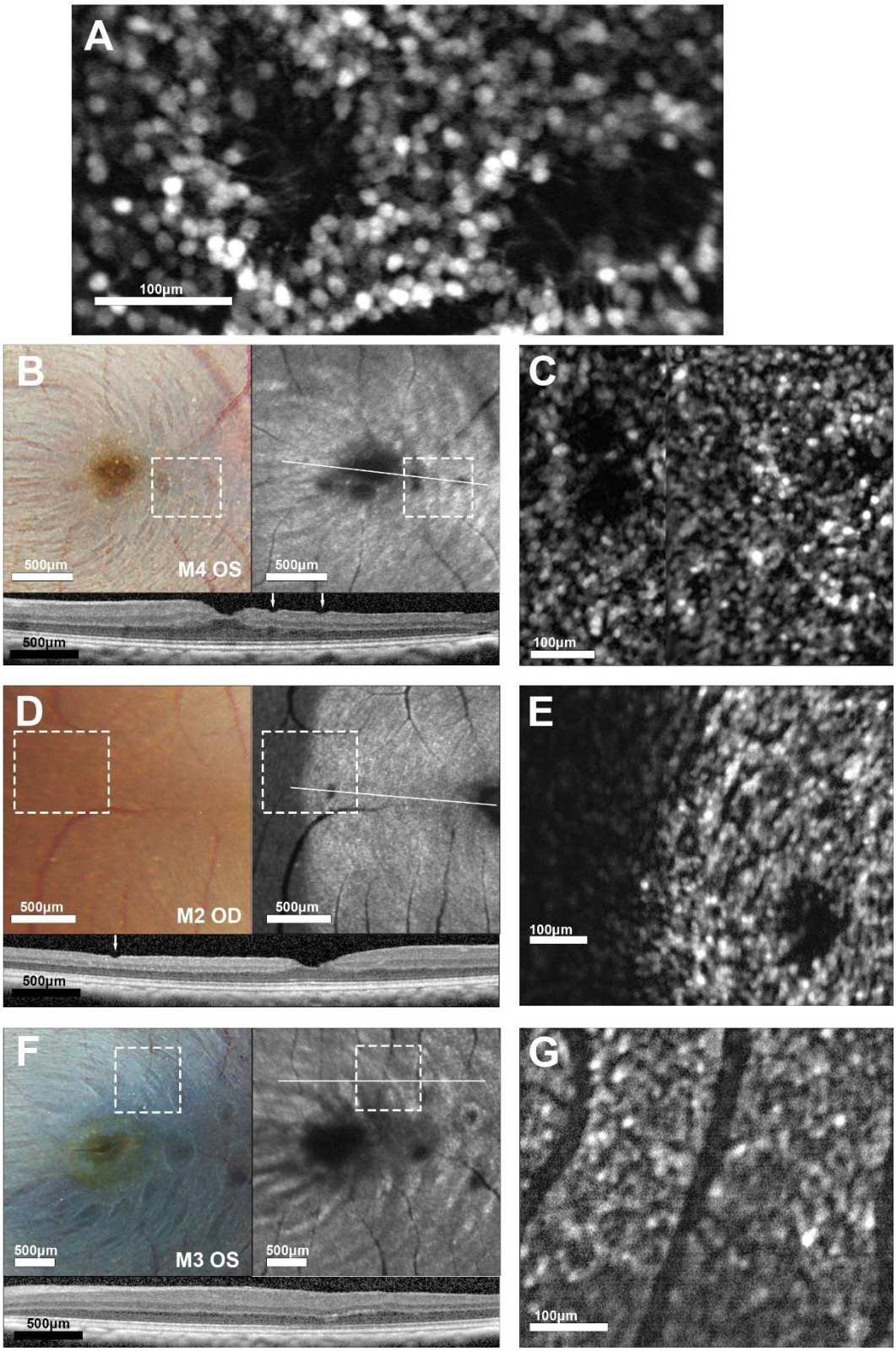
A
100µm
B
500µm
M4 OS
500µm
500µm
C
100µm
D
500µm
M2 OD
500µm
500µm
E
100µm
F
500µm
M3 OS
500µm
500µm
G
100µm

Figure 7

A. AOSLO calcium image of two hypofluorescent areas in M3 OS. Dendrites are visible in these regions. **B.** Color fundus (top-left) and cSLO BAF (top-right) of M3 OS showing two hypofluorescent areas that are investigated with OCT (bottom). **C.** Montaged fluorescence AOSLO image reveals dimples in OCT correspond to the two areas in AOSLO. **D.** Color fundus location with no macular dark spots but a hypofluorescent region in the cSLO BAF **E.** OCT, and AOSLO of the hyperfluorescent region seen in D. **F.** Color fundus location with CMDS streaks but no visible RNFL dimples in OCT or **G.** hypofluorescent RGC expression in AOSLO.

Discussion

In this study, we evaluated the ILM peeling technique as a tool to enable widespread functional recording from the GCL in the living primate following viral transduction of GCaMP. First, we demonstrated an expanded area of GCaMP fluorescence in the eye following an ILM peel paired with an intravitreal injection. This is the first reported use of GCaMP8 for *in vivo* functional imaging of RGCs. Next, we recorded from the control and ILM peeled eyes over a period of 6 months to establish long-term efficacy. The procedure was then repeated successfully in an additional 4 eyes. Fundus photography and OCT revealed minor morphological changes in the retina; in addition to changes in the foveal contour AOSLO and OCT confirmed the absence of RGCs in small pockets along. We considered this minimal loss of RGCs acceptable tradeoff given the greatly expanded region for calcium imaging *in vivo.*

ILM peel enables functional imaging of RGCs beyond the fovea in the living eye

By utilizing an ILM peel approach to expand the area of RGCs transduced by a viral vector coding for the calcium indicator GCaMP we successfully recorded from retinal ganglion cells *in vivo* from all eyes to an average of 8.5 degrees eccentricity, an area that would have been inaccessible using standard methods. By extending functional imaging beyond the fovea, we can potentially access a more diverse range of retinal ganglion cell types that may occur more infrequently or are specialized for non-foveal functions. In M1, we both compared the responsivity of RGCs at comparable eccentricities with a control eye and followed two retinal locations up to six months post ILM peel. We observed no significant differences in group Z scores and no significant decrease in RGC responsiveness over the observation period, suggesting that retinal function was not compromised by the surgical procedure.

Given the potentially variable surgical outcomes and variations in immune reaction amongst different individuals, we repeated this experiment in an additional four macaque eyes. One general trend amongst all eyes was a decrease in z-score responsiveness and sparser labeling as foveal eccentricity increased. A higher z-score at central eccentricities may be due the inability of AOSLO to axially separate overlapping RGCs at the fovea where ganglion cell densities are higher (Curcio and Allen 1990).

Subject M1 responded with significantly higher z-scores relative to other experimental eyes, which could be attributed to the older age of that animal a factor that has a profound impact on innate immunity and potentially therefore on viral transduction. M1 also had a much shorter time between ILM peel and the first intravitreal injection, minimizing any potential obstruction of viral access to the GCL by retinal glia mediated scar formation. The levels of inactivating antibodies for AAV2 (table 1) may affect transduction, but this alone was not sufficient in explaining the disparity with M2 who had similar inactivating antibody levels.

Functional responses can be obtained from the retinal nerve fiber layer *in vivo*

Functional assessment of responses carried along RGC axons rather than recorded directly from RGC somas was possible beyond the ILM peel as shown in figure 4. This allowed coarse extraction of RGC activity sent to the optic nerve. We note that the RNFL trace was dominated by an OFF response that may be explained by the stimulus design. A high photopic mean light level can drive stronger OFF responses than ON. We also observed that the ILM peeled eye responded at twice the z-score of the control eye, this could be explained by the increased number of GCaMP-expressing RGCs in the ILM peeled eye. An enlarged pan retinal stimulus could further increase the measured RNFL response by activating additional RGCs. This finding raises the possibility of RGC responses being contaminated by the overlying RNFL, but fortunately the somas dominate the GCaMP signal. For this same reason, RGC somas make it difficult to focus on the RNFL unless recordings are made beyond the edge of the ILM peel. Recording directly from the RNFL may be of interest for pre-clinical models of glaucoma or assessing axon regeneration of transplanted ganglion cells *in vivo* (de Lima 2012).

The ocular inflammation associated with viral vector injections is not dramatically increased by ILM peel in immune suppressed animals.

A board-certified ophthalmologist evaluated ocular inflammation following intravitreal injection of the viral vector based on a modified Hackett-McDonald scoring system (Supplementary Table 1) [29]. We observed variability between animals with overall inflammation scores for both eyes of M2 greater than M3 both before and after viral vector injection. Inflammation was characterized principally by conjunctival congestion, swelling, and decreased corneal transparency with an additional note of pigment on the anterior capsule of OS. M3 experienced a similar decrease in corneal transparency to M2 but relatively little

conjunctival congestion and swelling, as well as faster reduction in inflammation score following injection. Despite this inflammation, viable expression was seen in all eyes for the duration of this study. Interestingly there was no statistically significant difference in cell responsivity between the initially injected and fellow eyes despite literature suggesting a rapid increase in inactivating antibodies that can jeopardize transduction of the fellow eye ((Yin et al. 2011; Li et al. 2008)). This may have been a result of using immune suppression.

In the small numbers of animals in this study, peeling the ILM prior to intravitreal injection of the viral vector did not trigger substantially more inflammation relative to the standard procedure. Compared to a comparably immune suppressed animal that received intravitreal injection of AAV2:CAG:GCaMP6s in a non-vitrectomized eye with no ILM peel (McGregor et al. 2022), M2 scored higher in overall inflammatory response while M3 had a lower score. Both M2 and M3 recovered faster than this comparable animal although it is important to note that there were small differences in the viral vector between these two studies; here we used a ganglion cell specific promoter SNCG (Chaffiol et al. 2017) with a 7m8 (Dalkara et al. 2013) serotype whereas CAG was used previously with AAV2. The GCaMP generations were also different. Further work is needed to definitively conclude ILM peel prior to injection does not lead to more inflammation, particularly given the variability between animals, but we did not observe a dramatic increase in inflammation, suggesting that ILM peeling is a viable approach.

Surgical Outcomes associated with peeling the ILM

While the ILM peeling technique may open many new possibilities, careful consideration of the impact on the retina is warranted. The ILM is composed of muller cell foot plates whose removal following an ILM peel may cause muller cell dysfunction (Gandorfer et al. 2001). Studies have found that although the ILM does not regrow, muller cells produce a basement membrane from

their processes that cover most of the retina except in some areas due to errors during wound healing (Hisatomi et al. 2014). The first typical complication seen in the eye, not seen in our results due to short timescale, is swelling of arcuate RNFL that appears hyporeflective in structural imaging (Díaz-Valverde and Wu 2018). We do observe altered foveal contours in some cases, as seen in figure 6 and this is a common surgical outcome in humans. Sparing the foveal center during the peel process may significantly improve the foveal contour for future experiments (Murphy et al. 2020) but it is important to note that outcomes related to ILM peeling in humans as a part of macular hole surgery may be different when applied to an otherwise healthy macaque eye.

Color fundus photography of M2 and M3 revealed numerous stretch marks traveling in the direction of the optic nerve, a feature consistent with disassociated optical nerve fiber layer (DONFL) first reported by Tadayoni in 2001 (Tadayoni et al. 2001; Christensen et al. 2009), also known as concentric macular dark spots (CMDS) (Alkabes et al. 2011), or inner retinal dimpling (Pichi et al. 2014). DONFL is more frequently observed in temporal retina, where the RNFL is thinner compared to the nasal side (Nukada et al. 2013).

High resolution imaging revealed several scattered hypofluorescent pockets in the ganglion cell layer corresponding to round defects in the fundus and cSLO along with dimples in the OCT (Figure 7**)**. All AOSLO observations of these structures are spatially restricted to no more than 100um in diameter. This is the first time that disruption to the ganglion cell layer has been shown in vivo at a cellular scale. Previous immunohistochemical studies found that excised ILM contained RGCs, suggesting that they are being lost during the ILM peel process (La Heij et al. 2005), and other studies have reported dimples consistent with localized ganglion cell loss in OCT (Baba et al. 2012). We note that ganglion cell loss is restricted to small round defects rather than the regions of DONFL (Figure 7F). These previously reported round retinal defects appear around the macula and are covered by glia, though damage to the RGC layer

has been unclear (Hisatomi et al. 2017). Relative to the advantage offered dramatically more widespread GCaMP expression we feel these limited pockets of ganglion cell loss are tolerable, particularly as there location is clear.

Alternative methods to circumvent the restricted viral transduction imposed by the ILM in primates have been suggested including enzymatic digestion of the ILM with a nonspecific protease (Dalkara et al. 2009; Zhang, Tuffy, et al. 2021), photodisruption (Peynshaert et al. 2022; Janknecht et al. 2001) or sub-ILM injection (Boye et al. 2016). Enzymatic digestion has the advantage of not requiring surgery, but this has not been attempted in NHPs where the ILM is thicker than in small animal models. As ILM thickness is eccentricity dependent in primates, it is not straightforward to titrate the correct dose, risking substantial retinal damage. Photodisruption is a novel technique that has been tested successfully in bovine retinal explants (Peynshaert et al. 2022) using indocyanine green and a nanosecond laser protocol to form vapor nanobubbles that disrupt the ILM. Recently this work has been extended to an *in vivo* rabbit model (De Clerck et al. 2023), but more work still needs to be done before it can be applied to NHP. Lastly an alternative surgical strategy is the sub-ILM injection. A bleb is created beneath the ILM for delivery of the viral vector keeping more of the structure intact. This is surgically very challenging given the thickness of the ILM and there is a risk of delivering the viral vector sub-retinally or sub-hyloid, neither of which would target the GCL.

Conclusions

This study demonstrates not only that the ILM peel approach allows functional recording from a larger area of the GCL but also that the recordings remain stable over time and are comparable to those in eyes with no ILM peel. As such, this technique may be of value for pre-clinical evaluation of retinal function, both for detecting vision loss and assessing the impact of therapeutic interventions. For cell-based therapies where single cell resolution is

needed, a larger area to assess retinal function would greatly increase the chance of success given the potential sparse integration and uncertainty of the locus of cell delivery.

Supplementary Materials

Supplementary Table 1: Inflammation following intravitreal injection of the viral vector in all animals was scored longitudinally by a masked board certified ophthalmologist based on a modified Hackett-McDonald scoring system (Munger 2002). The assessment included slit lamp examination and observations of pupillary response and dilation. Scores shown are integrated from the 9 numerical measures listed in the attached Modified Hackett scoring sheet.

	Weeks post injection																
Animal	**-4**	**-3**	**-2**	**-1**	**0**	**1**	**2**	**3**	**4**	**5**	**6**	**7**	**8**	**9**	**10**	**11**	**12**
M2 OS							11		4		3	3	4		2		2
M2 OD	2		4			8	2		3		2					0	
M3 OS		2				0	4	4	2	3		2					
M3 OD	2					3	2	2		2							

References

Aboualizadeh, E., M. J. Phillips, J. E. McGregor, D. A. DiLoreto, Jr., J. M. Strazzeri, K. R. Dhakal, B. Bateman, L. D. Jager, K. L. Nilles, S. A. Stuedemann, A. L. Ludwig, J. J. Hunter, W. H. Merigan, D. M. Gamm, and D. R. Williams. 2020. 'Imaging Transplanted Photoreceptors in Living Nonhuman Primates with Single-Cell Resolution', *Stem Cell Reports*, 15: 482-97.

Alkabes, M., C. Salinas, L. Vitale, A. Bures-Jelstrup, P. Nucci, and C. Mateo. 2011. 'En face optical coherence tomography of inner retinal defects after internal limiting membrane peeling for idiopathic macular hole', *Invest Ophthalmol Vis Sci*, 52: 8349-55.

Baba, T., S. Yamamoto, R. Kimoto, T. Oshitari, and E. Sato. 2012. 'Reduction of thickness of ganglion cell complex after internal limiting membrane peeling during vitrectomy for idiopathic macular hole', *Eye*, 26: 1173-80.

Baron, W. S. 1973. 'Maxwellian view stimulator for electrophysiological or psychophysical work', *Appl Opt*, 12: 2560-2.

Batabyal, S., S. Gajjeraman, S. Pradhan, S. Bhattacharya, W. Wright, and S. Mohanty. 2021. 'Sensitization of ON-bipolar cells with ambient light activatable multi-characteristic opsin rescues vision in mice', *Gene Therapy*, 28: 162-76.

Boye, S. E., J. J. Alexander, C. D. Witherspoon, S. L. Boye, J. J. Peterson, M. E. Clark, K. J. Sandefer, C. A. Girkin, W. W. Hauswirth, and P. D. Gamlin. 2016. 'Highly Efficient Delivery of Adeno-Associated Viral Vectors to the Primate Retina', *Hum Gene Ther*, 27: 580-97.

Brooks, H. Logan. 2000. 'Macular hole surgery with and without internal limiting membrane peeling', *Ophthalmology*, 107: 1939-48.

Chaffiol, A., R. Caplette, C. Jaillard, E. Brazhnikova, M. Desrosiers, E. Dubus, L. Duhamel, E. Mace, O. Marre, P. Benoit, P. Hantraye, A. P. Bemelmans, E. Bamberg, J. Duebel, J. A. Sahel, S. Picaud, and D. Dalkara. 2017. 'A New Promoter Allows Optogenetic Vision Restoration with Enhanced Sensitivity in Macaque Retina', *Mol Ther*, 25: 2546-60.

Christensen, U. C., K. Kroyer, B. Sander, M. Larsen, V. Henning, J. Villumsen, and M. la Cour. 2009. 'Value of internal limiting membrane peeling in surgery for idiopathic macular hole stage 2 and 3: a randomised clinical trial', *British Journal of Ophthalmology*, 93: 1005-15.

Comander, Jason, Livia S Carvalho, Ru Xiao, Aliete Langsdorf, Sarah Wassmer, Brian Hafler, David M Wu, Dean Eliott, Leo A Kim, and Luk H Vandenberghe. 2016. 'Characterization of the limitations to gene transfer and associated inflammation following intravitreal AAV injection in nonhuman primates', *Investigative Ophthalmology & Visual Science*, 57: 771-71.

Curcio, Christine A., and Kimberly A. Allen. 1990. 'Topography of ganglion cells in human retina', *Journal of Comparative Neurology*, 300: 5-25.

Dalkara, D., L. C. Byrne, R. R. Klimczak, M. Visel, L. Yin, W. H. Merigan, J. G. Flannery, and D. V. Schaffer. 2013. 'In vivo-directed evolution of a new adeno-associated virus for therapeutic outer retinal gene delivery from the vitreous', *Sci Transl Med*, 5: 189ra76.

Dalkara, D., K. D. Kolstad, N. Caporale, M. Visel, R. R. Klimczak, D. V. Schaffer, and J. G. Flannery. 2009. 'Inner limiting membrane barriers to AAV-mediated retinal transduction from the vitreous', *Mol Ther*, 17: 2096-102.

De Clerck, Kaat, Helena Vanluchene, Kevin Braeckmans, Stefaan De Smedt, Katrien Remaut, and Karen Peynshaert. 2023. 'Characterization of enhanced lipid nanoparticle delivery after photodisruption of the inner limiting membrane', *Investigative Ophthalmology & Visual Science*, 64: 2614-14.

de Lima, S. 2012. 'Full-length axon regeneration in the adult mouse optic nerve and partial recovery of simple visual behaviors (vol 109, pg 9149, 2012)', *Proceedings of the National Academy of Sciences of the United States of America*, 109: 13465-65.

Dera, Adrianna U., Doerte Stoll, Verena Schoeneberger, Marcus Walckling, Claudia Brockmann, Thomas A. Fuchsluger, and Friederike Schaub. 2023. 'Anatomical and functional results after vitrectomy with conventional ILM peeling versus inverted ILM flap technique in large full-thickness macular holes', *International Journal of Retina and Vitreous*, 9: 68.

Díaz-Valverde, Andrea, and Lihteh Wu. 2018. 'TO PEEL OR NOT TO PEEL THE INTERNAL LIMITING MEMBRANE IN IDIOPATHIC EPIRETINAL MEMBRANES', *RETINA*, 38.

Ferrari, U., S. Deny, A. Sengupta, R. Caplette, F. Trapani, J. A. Sahel, D. Dalkara, S. Picaud, J. Duebel, and O. Marre. 2020. 'Towards optogenetic vision restoration with high resolution', *PLoS Comput Biol*, 16: e1007857.

Gandorfer, Arnd, Christos Haritoglou, Carolin A. Gass, Michael W. Ulbig, and Anselm Kampik. 2001. 'Indocyanine green-assisted peeling of the internal limiting membrane may cause retinal damage', *American Journal of Ophthalmology*, 132: 431-33.

Ganjawala, T. H., Q. Lu, M. D. Fenner, G. W. Abrams, and Z. H. Pan. 2019. 'Improved CoChR Variants Restore Visual Acuity and Contrast Sensitivity in a Mouse Model of Blindness under Ambient Light Conditions', *Molecular Therapy*, 27: 1195-205.

Gauvain, G., H. Akolkar, A. Chaffiol, F. Arcizet, M. A. Khoei, M. Desrosiers, C. Jaillard, R. Caplette, O. Marre, S. Bertin, C. M. Fovet, J. Demilly, V. Forster, E. Brazhnikova, P. Hantraye, P. Pouget, A. Douar, D. Pruneau, J. Chavas, J. A. Sahel, D. Dalkara, J. Duebel, R. Benosman, and S. Picaud. 2021. 'Optogenetic therapy: high spatiotemporal resolution and pattern discrimination compatible with vision restoration in non-human primates', *Communications Biology*, 4.

Godat, T., N. P. Cottaris, S. Patterson, K. Kohout, K. Parkins, Q. Yang, J. M. Strazzeri, J. E. McGregor, D. H. Brainard, W. H. Merigan, and D. R. Williams. 2022. 'In vivo chromatic and spatial tuning of foveolar retinal ganglion cells in Macaca fascicularis', *PLoS One*, 17: e0278261.

Gray, D. C., W. Merigan, J. I. Wolfing, B. P. Gee, J. Porter, A. Dubra, T. H. Twietmeyer, K. Ahamd, R. Tumbar, F. Reinholz, and D. R. Williams. 2006. 'In vivo fluorescence imaging of primate retinal ganglion cells and retinal pigment epithelial cells', *Optics Express*, 14: 7144-58.

Hammer, J., P. Roeppenack, S. Yousuf, C. Schnabel, A. Weber, D. Zoeller, E. Koch, S. Hans, and M. Brand. 2022. 'Visual Function is Gradually Restored During Retina Regeneration in Adult Zebrafish', *Frontiers in Cell and Developmental Biology*, 9.

Hisatomi, T., S. Notomi, T. Tachibana, Y. Sassa, Y. Ikeda, T. Nakamura, A. Ueno, H. Enaida, T. Murata, T. Sakamoto, and T. Ishibashi. 2014. 'Ultrastructural changes of the vitreoretinal interface during long-term follow-up after removal of the internal limiting membrane', *Am J Ophthalmol*, 158: 550-6.e1.

Hisatomi, Toshio, Takashi Tachibana, Shoji Notomi, Shunji Nakatake, Kohta Fujiwara, Yusuke Murakami, Yasuhiro Ikeda, Shigeo Yoshida, Hiroshi Enaida, Toshinori Murata, Taiji Sakamoto, Koh-Hei Sonoda, and Tatsuro Ishibashi. 2017. 'INCOMPLETE REPAIR OF RETINAL STRUCTURE AFTER VITRECTOMY WITH INTERNAL LIMITING MEMBRANE PEELING', *RETINA*, 37: 1523-28.

Janknecht, P., N. Feltgen, T. Wesendahl, J. Wiek, B. Eissner, B. Ott, F. Staubach, and M. Frenz. 2001. 'Internal limiting membrane ablation in pig eyes with the Er:YAG laser under perfluorodecalin', *Graefes Arch Clin Exp Ophthalmol*, 239: 705-11.

La Heij, Ellen C., Suzanne C. Dieudonné, Cornelia M. Mooy, Roselie M. H. Diederen, Albert T. A. Liem, Robert J. van Suylen, and Fred Hendrikse. 2005. 'Immunohistochemical Analysis of the Internal Limiting Membrane Peeled With Infracyanine Green', *American Journal of Ophthalmology*, 140: 1123-25.

Leffler, Joseph, Melody Hernandez, Kang-Chieh Huang, Cátia Gomes, Aristomenis Thanos, Grant Cull, Michaela Dunn, Priya Chaudhary, Subramanian Dharmarajan, Gareth Howell, Yvonne Ou, Brad Fortune, Jason S. Meyer, and Benjamin Sivyer. 2023. 'Towards the optimization of human stem cell-derived RGC integration in glaucomatous non-human primate retina', *Investigative Ophthalmology & Visual Science*, 64: 4696-96.

Li, Q., R. Miller, P. Y. Han, J. Pang, A. Dinculescu, V. Chiodo, and W. W. Hauswirth. 2008. 'Intraocular route of AAV2 vector administration defines humoral immune response and therapeutic potential', *Mol Vis*, 14: 1760-9.

Lingam, S., Z. P. Liu, B. X. Yang, W. Wong, B. H. Parikh, J. Y. Ong, D. Goh, D. S. L. Wong, Q. S. W. Tan, G. S. W. Tan, G. E. Holder, K. Regha, V. A. Barathi, W. Hunziker, G. Lingam, X. M. Zeng, and X. Y. Su. 2021. 'cGMP-grade human iPSC-derived retinal photoreceptor precursor cells rescue cone photoreceptor damage in non-human primates', *Stem Cell Research & Therapy*, 12.

Lu, Q., T. H. Ganjawala, S. Hattar, G. W. Abrams, and Z. H. Pan. 2018. 'A Robust Optomotor Assay for Assessing the Efficacy of Optogenetic Tools for Vision Restoration', *Investigative Ophthalmology & Visual Science*, 59: 1288-94.

Mathieson, K., J. Loudin, G. Goetz, P. Huie, L. Wang, T. I. Kamins, L. Galambos, R. Smith, J. S. Harris, A. Sher, and D. Palanker. 2012. 'Photovoltaic Retinal Prosthesis with High Pixel Density', *Nat Photonics*, 6: 391-97.

McGregor, J. E., T. Godat, K. R. Dhakal, K. Parkins, J. M. Strazzeri, B. A. Bateman, W. S. Fischer, D. R. Williams, and W. H. Merigan. 2020. 'Optogenetic restoration of retinal ganglion cell activity in the living primate', *Nat Commun*, 11: 1703.

McGregor, J. E., L. Yin, Q. Yang, T. Godat, K. T. Huynh, J. Zhang, D. R. Williams, and W. H. Merigan. 2018. 'Functional architecture of the foveola revealed in the living primate', *PLoS One*, 13: e0207102.

McGregor, Juliette E., Karteek Kunala, Zhengyang Xu, Peter J. Murphy, Tyler Godat, Jennifer M. Strazzeri, Brittany A. Bateman, William S. Fischer, Keith Parkins, Colin J. Chu, Teresa Puthussery, David R. Williams, and William H. Merigan. 2022. 'Optogenetic therapy restores retinal activity in primate for at least a year following photoreceptor ablation', *Molecular Therapy*, 30: 1315-28.

Munger, R. J. 2002. 'Veterinary ophthalmology in laboratory animal studies', *Vet Ophthalmol*, 5: 167-75.

Murphy, Declan C., Will Fostier, Jon Rees, and David H. Steel. 2020. 'FOVEAL SPARING INTERNAL LIMITING MEMBRANE PEELING FOR IDIOPATHIC MACULAR HOLES: EFFECTS ON ANATOMICAL RESTORATION OF THE FOVEA AND VISUAL FUNCTION', *RETINA*, 40.

Nikonov, S., P. Aravand, A. Lyubarsky, R. Nikonov, A. J. Luo, Z. Y. Wei, A. M. Maguire, N. T. Phelps, I. Shpylchak, K. Willett, T. S. Aleman, R. M. Huckfeldt, P. S. Ramachandran, and J. Bennett. 2022. 'Restoration of Vision and Retinal Responses After Adeno-Associated Virus-Mediated Optogenetic Therapy in Blind Dogs', *Translational Vision Science & Technology*, 11.

Nukada, K., M. Hangai, S. Ooto, M. Yoshikawa, and N. Yoshimura. 2013. 'Tomographic features of macula after successful macular hole surgery', *Invest Ophthalmol Vis Sci*, 54: 2417-28.

Palanker, D., Y. Le Mer, S. Mohand-Said, M. Muqit, and S. Jose. 2020. 'Photovoltaic Restoration of Central Vision in Atrophic Age-Related Macular Degeneration', *Ophthalmology*, 127: 1097-104.

Peynshaert, Karen, Helena Vanluchene, Kaat De Clerck, An-Katrien Minnaert, Morgane Verhoeven, Noémie Gouspillou, Nezahat Bostan, Toshio Hisatomi, Geraldine Accou, Félix Sauvage, Kevin Braeckmans, Stefaan De Smedt, and Katrien Remaut. 2022. 'ICG-mediated photodisruption of the inner limiting membrane enhances retinal drug delivery', *Journal of Controlled Release*, 349: 315-26.

Pichi, Francesco, Andrea Lembo, Mariachiara Morara, Chiara Veronese, Micol Alkabes, Paolo Nucci, and Antonio P. Ciardella. 2014. 'Early and late inner retinal changes after inner limiting membrane peeling', *International Ophthalmology*, 34: 437-46.

Roorda, A., F. Romero-Borja, W. J. Donnelly, H. Queener, T. J. Hebert, and M. C. W. Campbell. 2002. 'Adaptive optics scanning laser ophthalmoscopy', *Optics Express*, 10: 405-12.

Rossi, E. A., P. Rangel-Fonseca, K. Parkins, W. Fischer, L. R. Latchney, M. A. Folwell, D. R. Williams, A. Dubra, and M. M. Chung. 2013. 'In vivo imaging of retinal pigment epithelium cells in age related macular degeneration', *Biomed Opt Express*, 4: 2527-39.

Tadayoni, R., M. Paques, P. Massin, S. Mouki-Benani, J. Mikol, and A. Gaudric. 2001. 'Dissociated optic nerve fiber layer appearance of the fundus after idiopathic epiretinal membrane removal', *Ophthalmology*, 108: 2279-83.

Takahashi, Kazuhisa, Tsutomu Igarashi, Koichi Miyake, Maika Kobayashi, Chiemi Yaguchi, Osamu Iijima, Yoshiyuki Yamazaki, Yuko Katakai, Noriko Miyake, Shuhei Kameya, Takashi Shimada, Hiroshi Takahashi, and Takashi Okada. 2017. 'Improved Intravitreal AAV-Mediated Inner Retinal Gene Transduction after Surgical Internal Limiting Membrane Peeling in Cynomolgus Monkeys', *Molecular Therapy*, 25: 296-302.

Teo, Kelvin, Shu Yen Lee, and Ian Constable. 2018. 'The effect of Surgical removal of the Internal Limiting Membrane on AAV vector delivery to the Retina in a Non-Human Primate model', *Investigative Ophthalmology & Visual Science*, 59: 5660-60.

Teo, Kelvin Yi Chong, Shu Yen Lee, Amutha Veluchamy Barathi, Sai Bo Bo Tun, Licia Tan, and Ian Jeffery Constable. 2018. 'Surgical Removal of Internal Limiting Membrane and Layering of AAV Vector on the Retina Under Air Enhances Gene Transfection in a Nonhuman Primate', *Investigative Ophthalmology & Visual Science*, 59: 3574-83.

Thomas, R. J., B. A. Rockwell, W. J. Marshall, R. C. Aldrich, M. F. Gorschboth, S. A. Zimmerman, and R. J. Rockwell. 2007. 'Procedure for the computation of hazards from diffusely scattering surfaces under the Z136.1-2000 American National Standard for Safe Use of Lasers', *Journal of Laser Applications*, 19: 46-54.

Yang, Q., J. Zhang, K. Nozato, K. Saito, D. R. Williams, A. Roorda, and E. A. Rossi. 2014. 'Closed-loop optical stabilization and digital image registration in adaptive optics scanning light ophthalmoscopy', *Biomed Opt Express*, 5: 3174-91.

Yin, L., K. Greenberg, J. J. Hunter, D. Dalkara, K. D. Kolstad, B. D. Masella, R. Wolfe, M. Visel, D. Stone, R. T. Libby, D. DiLoreto, D. Schaffer, J. Flannery, D. R. Williams, and W. H. Merigan. 2011. 'Intravitreal Injection of AAV2 Transduces Macaque Inner Retina', *Investigative Ophthalmology & Visual Science*, 52: 2775-83.

Yin, Lu, Benjamin Masella, Deniz Dalkara, Jie Zhang, John. G. Flannery, David V. Schaffer, David R. Williams, and William H. Merigan. 2014. 'Imaging Light Responses of Foveal Ganglion Cells in the Living Macaque Eye', *The Journal of Neuroscience*, 34: 6596-605.

Zhang, H., B. Su, L. Jiao, Z. H. Xu, C. J. Zhang, J. Nie, M. L. Gao, Y. V. Zhang, and Z. B. Jin. 2021. 'Transplantation of GMP-grade human iPSC-derived retinal pigment epithelial cells in rodent model: the first pre-clinical study for safety and efficacy in China', *Ann Transl Med*, 9: 245.

Zhang, K. Y., C. Tuffy, J. L. Mertz, S. Quillen, L. Wechsler, H. A. Quigley, D. J. Zack, and T. V. Johnson. 2021. 'Role of the Internal Limiting Membrane in Structural Engraftment and Topographic Spacing of Transplanted Human Stem Cell-Derived Retinal Ganglion Cells', *Stem Cell Reports*, 16: 149-67.

Zhang, Y., M. Rozsa, Y. Liang, D. Bushey, Z. Wei, J. Zheng, D. Reep, G. J. Broussard, A. Tsang, G. Tsegaye, S. Narayan, C. J. Obara, J. X. Lim, R. Patel, R. Zhang, M. B. Ahrens, G. C. Turner, S. S. Wang, W. L. Korff, E. R. Schreiter, K. Svoboda, J. P. Hasseman, I. Kolb, and L. L. Looger. 2023. 'Fast and sensitive GCaMP calcium indicators for imaging neural populations', *Nature*, 615: 884-91.